doi:10.1016/j.jmb.2004.01.028 J. Mol. Biol. (2004) 337, 255–261

JMB

Available online at www.sciencedirect.com

SCIENCE DIRECT®

ELSEVIER

Bending Stiffness of a Crystalline Actin Bundle

Jennifer H. Shin[1], L. Mahadevan[2]*, P. T. So[1] and Paul Matsudaira[3]

[1]*Department of Mechanical Engineering, M.I.T. Cambridge, MA 02139, USA*

[2]*Division of Engineering and Applied Sciences Harvard University, Pierce 324 Cambridge, MA 02138, USA*

[3]*Department of Biology Division of Biological Engineering, M.I.T. and Whitehead Institute Cambridge, MA 02142, USA*

**Corresponding author*

The acrosomal process of the sperm of the horseshoe crab (*Limulus polyphemus*) is a unique crystalline actin bundle, consisting of multiple actin filaments cross-linked by the actin-bundling protein, scruin. For successful fertilization, the acrosomal bundle must penetrate through a 30 μm thick jelly coat surrounding the egg and thus it must be sufficiently stiff. Here, we present two measurements of the bending stiffness of a single crystalline bundle of actin. Results from these measurements indicate that the actin:scruin composite bundle has an average elastic modulus of 2 GPa, which is similar to that of a single actin filament, and a bending stiffness that is more than two orders of magnitude larger than that of a bundle of uncross-linked actin filaments due to stiffening by the scruin matrix.

Keywords: actin bundle; bending stiffness; single pole magnetic trap; tapering rod

Introduction

Actin filaments, which play an important role in maintaining the mechanical integrity of eukaryotic cells, rarely exist independently. Instead, they normally associate into bundles or networks in concert with more than 60 different actin-binding proteins (ABPs) to influence cellular shape, mitotic division, cell adhesion, and motility.[1] While the filaments form a disordered structure in networks, they form compact ordered arrays with relatively rigid proteins that force the close alignment in bundles. Examples of these stiff bundles are found in long thin processes such as the neuro-sensory bristle of *Drosophila*,[2–4] brush border microvilli,[5] hair cell stereocilia,[6,7] and the acrosomal process of *Limulus* sperm.[8,9] While the mechanical properties of actin in other states, especially the single-filament state[10,11] and the cross-linked gel state,[12,13] have been measured, we know of almost no mechanical property measurements on an individual crystalline bundle of multiple actin filaments; an important exception is the measurement of the bending stiffness of the actin hinge at the base of a hair cell.[14]

Here, we report the measurement of the bending stiffness of a crystalline bundle of actin found in the acrosomal process of the horseshoe crab *Limulus polyphemus* sperm (Figure 1). During fertilization, the coiled actin bundle extends from the sperm and penetrates the tough jelly coat of the egg (Figure 1). Recent work has shown that the bundle consists of actin filaments cross-linked by scruin:calmodulin heterodimers.[15] Since the bundle must be relatively stiff in bending for it to carry out its function, this system serves as a benchmark to understand the role of cross-linking in determining the mechanical properties in a macromolecular assembly. We use two independent methods for the measurement. In the first method, a steady transverse flow is used to deflect the acrosomal bundle and the bending stiffness is derived from an analysis of the equilibrium shape. The second method employs a single pole magnetic trap to bend the bundle and relate the deflection to the applied magnetic force, and thereby determine the bending stiffness.

Theory

Here, we outline the theoretical basis for the determination of the bending stiffness of the bundle from each of the experimental methods.

Hydrodynamic flow method

Electron micrographs of the acrosomal bundle reveal that the bundle is a non-prismatic rod of hexagonally packed and cross-linked actin

Abbreviation used: ASW, artificial seawater.

E-mail address of the corresponding author: lm@deas.harvard.edu

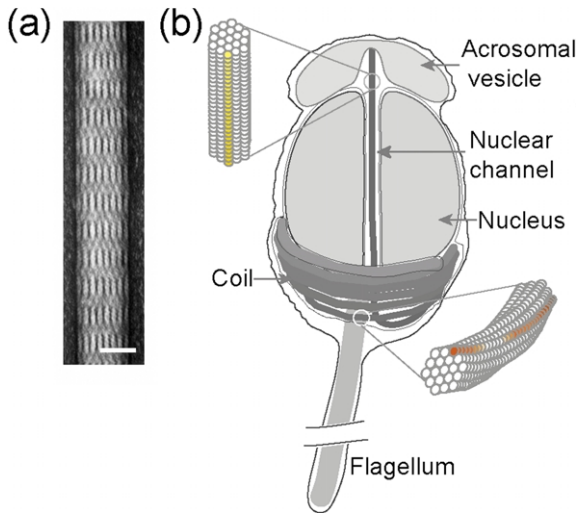

Figure 1. (a) An image of an isolated acrosomal bundle in the true discharge (TD) state taken from transmission electron microscopy. The scale bar represents 50 nm. (b) A schematic of unreacted *Limulus* sperm modified from electron micrographs, showing the proximal end of the acrosomal bundle lying in the nuclear channel while the rest of the bundle is coiled around the base of nucleus. Upon activation by the presence of an egg or Ca^{2+}, the acrosomal bundle uncoils and extrudes out of the acrosomal vesicle at a constant velocity. The blowups illustrate that the filaments are twisted in the coiled state, but parallel with each other in the TD state.

filaments with a continuously increasing radius from the tip to the base (15–80 filaments). For analysis, we assume the bundle to be a linearly tapering rod of length L and of radius $r(x)$. When a tapered elastic rod of stiffness $EI(x)$ is subject to a force per unit length f, its shape $y(x)$ for small deflection is determined by the solution of the differential equation:[15]

$$\frac{d^2}{dx^2}\left(EI(x)\frac{d^2y}{dx^2}\right) = f \tag{1}$$

In the presence of a steady flow, the Stokes drag per unit length for a long slender rod moving near a single plane wall is:[16]

$$f = 2\pi\mu\upsilon/\cosh^{-1}(h/R_{ave}) \tag{2}$$

Here, μ is the viscosity of the medium, υ the velocity of the flow, h the distance between the bundle and the wall, and R_{ave} the average radius of the bundle. The bundle is assumed to be clamped at the proximal end, consistent with observations, while the distal end is free of forces and moments. Therefore, the boundary conditions supplementing these are:[17]

$$y = 0,\ \frac{dy}{dx} = 0 \text{ at } x = 0 \tag{3}$$

$$\frac{d^2y}{dx^2} = 0,\ \frac{d^3y}{dx^3} = 0 \text{ at } x = L$$

One way to obtain the Young's modulus E using equation (1) is to find a polynomial fit to the experimental deflection curve and express E as a function of f and $I(x) = \pi/4(R_{min} + x\tan\beta)^4$ where R_{min} is the radius of the distal end and β is the taper angle. Unfortunately, this approach leads to large errors due to the sensitivity of the high-order polynomial fit to the experimental data and does not yield a reliable estimate of E.

To circumvent this difficulty, we model the bundle as a tapering segmented rod made of n cylinders whose radii, r_n, vary according to the linear function fitted to the slope of the bundle obtained from electron micrographs (Figure A1(a)). We assume each segment in the bundle to obey linear elastic theory, and apply the method of superposition to obtain the expression for the total deflection at the distal end, δ_{tot}, as a function of E, L, f, and $r_n(x)$ (see Appendix), and thus determine the Young's modulus E.

Magnetic trap method

In the case of magnetic trap measurements, a similar analysis can be performed with a point load $F_m = f\,\delta(x - L)$, where δ is the usual Dirac-delta function. Integrating equation (1) then leads to:

$$\frac{d}{dx}\left(EI_x\frac{d^2y}{dx^2}\right) = F_m \tag{4}$$

As in the previous case, we use the principle of superposition for a bundle composed of n cylinders ($1 \le n \le N$) to determine the total deflection $\delta_{tot} = \delta_1 + \delta_2 + \delta_3 + \ldots\delta_N$, and thence E (see Appendix).

Results and Discussions

Hydrodynamic flow method

Particle tracking is used to measure the flow velocity and confirm that it is steady. At least two particles lying in the plane of focus are chosen within a field of view to ensure that a uniform flow field exists. From equation (2), the force density applied to the deflecting bundle is calculated using $\mu = 10^{-3}$ Pa s, $h \sim 1$ μm, $R_{ave} = 46$ nm, and υ typically 45–120 μm/s from eight different cells. The measured tip deflection δ_{tot} ranges between 2.9 μm and 11.5 μm, validating the small deflection assumption used in deriving equation (1). As shown in Figure 2(c), the tip undergoes fluctuations about its average position at equilibrium. To minimize the uncertainty in the measurement, the displacement of the tip is averaged over 5–10 s. Figure 2(a) shows a typical deflection of the acrosome under the distributed load by a steady flow. The Young's modulus, E_{taper}, is obtained from equations (A1)–(A3) using the previously defined parameters and its averaged value over eight different cells is found to be

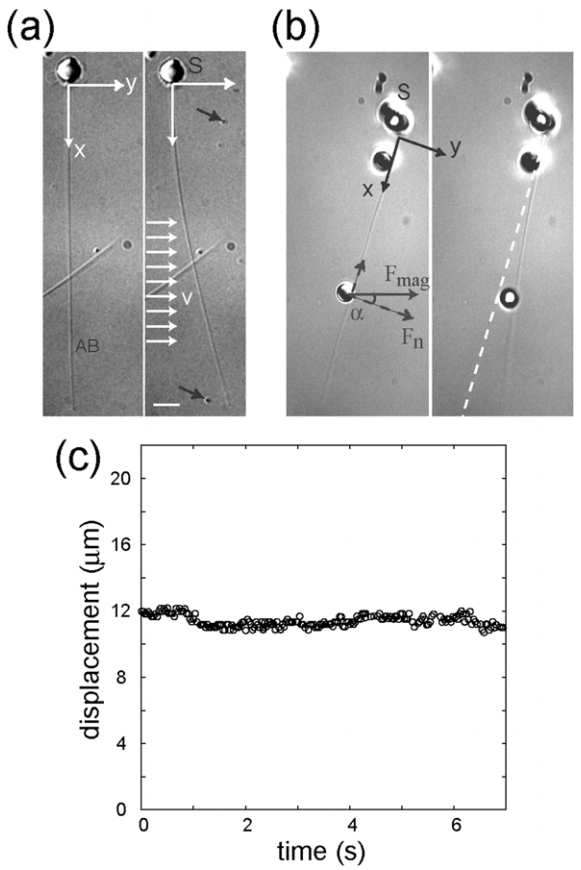

Figure 2. (a) DIC images of a bundle in the absence of and in the presence of a steady transverse flow. The black arrows locate the particles used to measure the flow velocity. S indicates sperm head and AB indicates the acrosomal bundle. The scale bar on the right panel represents 5 μm. (b) Images of the reacted sperm before and after the magnetic force is applied. Normal component of the force (to the long axis of the bundle) is calculated by taking cos α. (c) The bundle fluctuates about its average position at equilibrium; however, the data are averaged over 5–10 s to eliminate this effect.

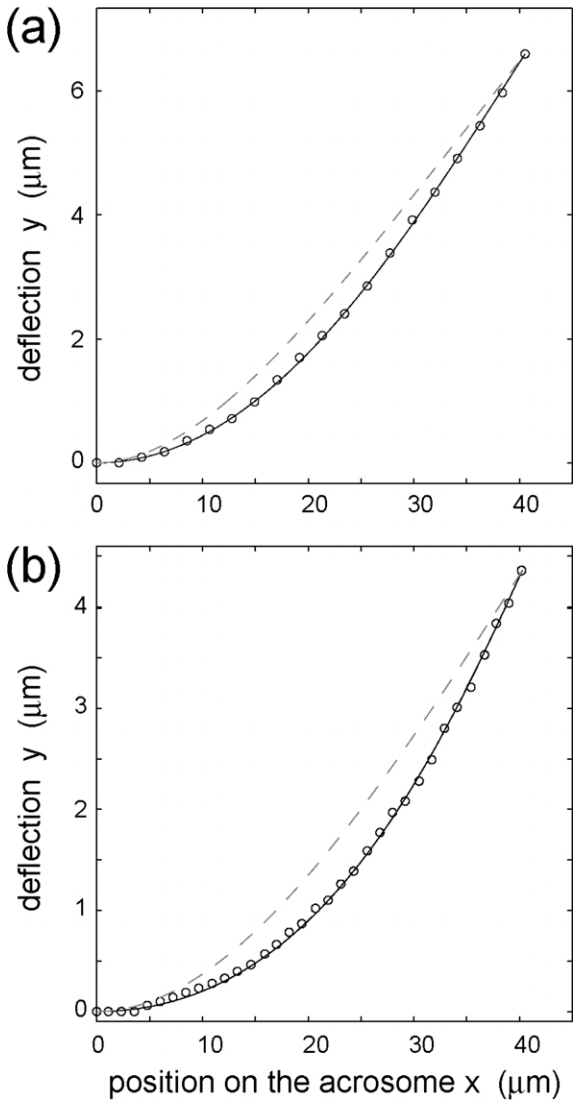

Figure 3. (a) Experimentally obtained shape of the deflected acrosomal bundle in steady hydrodynamic flow (open circle) is shown along with two analytical curves. The continuous line represents the theoretical curve using the tapered rod model, while the broken line represents the curve obtained by $y(x) = f(x^4 - 4x^3L + 6x^2L^2)/6\pi E_{ave}R_{ave}^4$ with the average value of E_{ave} assuming a uniform thickness rod. We define a goodness of the theoretical fit to the experimental data as: $\psi^2 = 1 - \frac{1}{N}\sum_{i=1}^{N}(y(x_i) - t(x_i)/y(x_i))^2$ where $y(x_i)$ is the experimental data, $t(x_i)$ the theoretically predicted value, and N the number of data along the curve, leading to $\psi^2_{taper} = 0.9984$ and $\psi^2_{uniform} = 0.8978$, with $\psi^2 = 1$ corresponding to a perfect fit. For this particular data, $E_{taper} = 2.2$ GPa, $E_{ave} = 2.3$ GPa, and the $EI_{ave} = 8 \times 10^{-21}$ N m^2. The distributed load density $f = 2.4 \times 10^{-7}$ N/m. (b) Experimental shape of the deflected acrosomal bundle with the point load, F_m, exerted by the magnetic field (open circle), along with two analytical curves. The continuous line represents the theoretical curve using the tapered rod model, while the broken line represents the theoretical curve for uniform thickness rod by $y(x) = 2F_m x^2(3a - x)/3\pi ER_{ave}^4$. For this particular data, $E_{taper} = 1.4$ GPa, $E_{ave} = 1.2$ GPa, and the $EI_{ave} = 4.1 \times 10^{-21}$ N m^2. The theoretical curve from the tapered model fits the experimental deflection well with $\psi^2_{taper} = 0.9967$, while the uniform rod model shows a large discrepancy with $\psi^2_{uniform} = 0.8228$.

$E_{taper} = 2.5(\pm 0.72)$ GPa. Since I, the moment of inertia, scales as the fourth power of r, EI rises from 0.9×10^{-21} N m^2 to 16×10^{-21} N m^2 for the estimated constant value of E_{taper}. The average bending stiffness of $\sim 5 \times 10^{-21}$ N m^2 corresponds to an average persistence length of $Lp = EI/k_BT \sim 1.2$ m, implying that the acrosome bundle is clearly impervious to thermal fluctuations over cellular dimensions. For comparison, we find that approximating the rod as a cylinder with a constant radius, R_{ave}, leads to $E_{ave} = 2.38(\pm 0.81)$ GPa using $E_{ave} = fL^4/(2\pi R_{ave}^4 \delta_{tot})$. Although the numerical value E_{ave} is not very different from E_{taper}, the tapering rod model leads to a shape that is much closer to the experimentally observed shape (Figure 3(a)).

Magnetic trap method

The single pole magnetic trap experiment provides us with an independent measurement of the

Table 1. Young's modulus (E) measurements at various voltages with the magnetic trap method

Voltage	5	10	15	20	25
$V \pm$ SD (μm/s)	1.3 ± 0.2	2.1 ± 0.1	3.5 ± 0.2	4.8 ± 0.6	8.9 ± 0.4
$F \pm$ SD (pN)	0.35 ± 0.05	0.56 ± 0.07	0.91 ± 0.05	1.25 ± 0.16	2.35 ± 0.02
$E \pm$ SD (GPa)	1.26 ± 0.62	1.18 ± 0.2	1.36 ± 0.15	1.58 ± 0.11	1.46 ± 0.1

To calibrate the forces at specified voltages, the velocities of 2.8 μm diameter magnetic beads moving in 4.95 M $CaCl_2$ solutions are measured. Since the maximum velocity (V) of the beads at the highest voltage does not exceed 9 μm/s, leading to a Reynolds number of 10^{-5}, the magnetic force (F) can be estimated directly from the drag force using the Stokes formula, $F_m = 6\pi\mu r_p \nu_m$, where μ is the viscosity of 4.95 M $CaCl_2$ solution, $\mu = 9.95 \times 10^{-3}$ Pa s, r_p the particle radius, and ν_m the particle velocity. The elastic modulus value (E) corresponding to each voltage is calculated from equation (A3).

bending stiffness. We calibrate the force following the analysis described by Amblard *et al.* by relating the magnetic field to the hydrodynamic forces on the beads suspended in a solution of 4.95 M $CaCl_2$.[18] Velocities are measured for beads located at least 30 μm from the bottom of the flow-cell to guarantee that wall effects are negligible and their values are given in Table 1. We first use Stokes formula, $F_m = 6\pi\mu r_p \upsilon_m$, to obtain the magnitude of the force. The perpendicular component of the force is $F_n = F_m \cos\alpha$, where α is the angle between the direction of the moving bead and the bundle axis (Figure 2(b)). With the values of $F_\perp$, δ_{tot}, and a, the distance between the attached magnetic bead on the acrosome and the base ($x = 0$), the mean elastic modulus is found to be $E_{taper} = 1.34(\pm 0.34)$ GPa from five different cells at all voltages, while the average bending stiffness EI varies from 0.37×10^{-21} Nm^2 to 10.6×10^{-21} Nm^2 from the tip to the base (Table 1). Figure 3(b) shows the theoretical fit to the experimentally obtained deflection.

A few potential sources for variation in the obtained results should be considered. First and most important, there are variations among individual sperm cells. A second likely source of variation lies in the inaccuracy associated with particle velocity measurements due to a finite optical depth-of-field, which can give rise to about two-fold variations in the flow velocity estimates. In addition, there could be an error associated with the estimate of the bundle taper.

We now consider the relation of the stiffness of the bundle to the stiffness of a single actin filament. Each bundle of acrosome consists of 15–80 filaments arranged along a tapering cross-section. If the acrosome bundle is assumed to be a rod of a uniform radius, $R_b \sim 50$ nm, made of 50 actin filaments cross-linked by scruin, the average stiffness $EI_{ave} \sim 8 \times 10^{-21}$Nm^2 corresponds to a material with Young's modulus of 2 GPa ($EI_{bundle} = E\pi R_b^4/4$). This value for Young's modulus is comparable with that of a stiff elastomer and similar to that of pure actin filaments (~2.6 GPa).[10,11] In contrast, if we suppose that we have a bundle of 50 uncross-linked actin filaments of radius r_f in a rope-like configuration, the stiffness of such a bundle $EI_{rope} = (E\pi r_f^4/4)n \sim 2.6 \times 10^{-23}$ Nm^2, where n is the number of filaments in the bundle. Therefore, the cross-linked actin bundle is more than 300 times stiffer than a braid/rope of uncross-linked actin filaments of a similar radius. This indicates that the presence of scruin is responsible for the large increase in the stiffness of the acrosome bundle. Electron micrographs lend some credence to our hypothesis; they show that there is a high density of scruin cross-links,[15] which allows for the substantial stiffening seen experimentally. Thus, the functional requirement for a stiff actin bundle required to penetrate the tough coat of the egg is well met by the stiffening induced by the tight cross-linker scruin.

Materials and Methods

Sample preparation

Horseshoe crab (*L. polyphemus*) sperm (500 μl) was collected from a healthy male and stored on ice. The collected sperm was washed at least twice in artificial seawater (ASW: 423 mM NaCl, 9 mM KCl, 9.27 mM $CaCl_2$, 22.94 mM $MgCl_2$, 25.5 mM $MgSO_4$, 2.15 mM $NaHCO_3$, 10 mM Tris, pH adjusted to 7.9–8.0) by centrifugation at 750*g* for five minutes, and resuspending in ASW to its original volume. Washed sperm were diluted 1:1000 (v/v) in ASW. The experiments were conducted in a flat capillary flow-cell constructed with pieces of coverslip and double-sided adhesive spacers, sealed with inert vacuum grease (Apiezon Co., Manchester, UK) to prevent leaking.

Activation of the acrosome reaction

The flow-cell was first freshly coated with a tissue adhesive, BIOBOND (Cat no. 71304, EMS, Inc, Fort Washington, PA), filled with diluted sperm, and incubated for about 10–20 minutes for secure adhesion to the surface of the coverslip. Saturated casein in ASW was diluted 100-fold with ASW, and several flow-cell volumes of the diluted solution were then added to the flow-cell to block the glass surface from non-specific binding of the extending acrosome and the beads used for flow visualization. After 20 minutes, the saturated casein solution was replaced with ASW containing 25 mM $CaCl_2$. Calcium ionophore (A23187, 2 mg/ml in ethanol) was diluted 1:10 (v/v) with ASW containing 25 mM $CaCl_2$. A small amount (20 μl) of the diluted ionophore was injected into the flow-cell to induce true discharge. Excess liquid was drawn from one side of the flow-cell as the diluted ionophore was pipetted into the other side.

Biotinylation of sperm cells

For the magnetic trap methods, streptavidin-coated magnetic beads (Dynabeads® M-280 streptavidin, Dynal Biotech, Inc. Cat no. 112.05) were attached to biotinylated sperm. Sulfo-NHS-LC Biotin was stored at −20 °C as a 10 mg/ml stock solution in anhydrous DMSO and diluted to 1:100 in ASWII. Sperm were washed twice in ASWII (423 mM NaCl, 9 mM KCl, 9.27 mM $CaCl_2$, 22.94 mM $MgCl_2$, 25.5 mM $MgSO_4$, 2.15 mM $NaHCO_3$, 10 mM Hepes, pH adjusted to 7.9–8.0). 10 μl of washed sperm (by centrifugation at 750*g* twice, for one minute each time) was added to 500 μl of prepared biotin solution. The sample was then incubated for two hours at room temperature on a rotating rack. Biotinylated sperm cells were then washed in regular ASW three times by centrifugation at 750*g*.

Measurement setup

The extended acrosome can be bent within a plane either by a flow of the buffer or by a magnetic force. The bending stiffness can then be calculated from an analysis of the equilibrium shape and deflection of the acrosome.

Hydrodynamic measurement

After fixing the sperm to a glass coverslip using BIO-BOND, the flow past the extended acrosomal bundle was induced inside the chamber by capillary absorption with filter-paper (No. 54 Hardened 90 mm Circles (Whatman, Inc., Clifton, NJ). Small polystyrene particles of diameter 0.175 μm were used to visualize the flow. The cells and the particles were imaged under DIC-H optics at a magnification of 100× on a Nikon TE300 inverted microscope, and these images were captured with a Dage MTI (model CD-300-RC, Dage-MTI, Inc., Michigan City, IN) video camera and recorded on a Sony SVO-9500MD S-VHS video cassette recorder. The velocity of flow was monitored using the trajectory of the particles travelling in the focal plane of the bundle. Selected video images were digitized at 30 frames/s using an Apple Video player. In addition, the still images of the acrosome bundle in the absence and in the presence of the steady flow were also captured to obtain the equilibrium shape (Figure 2(a)). We consider only the cases where the acrosomal bundle relaxes fully back to the initial position when the flow is removed.

Magnetic trap measurement

A focused load is applied to the bead-coupled bundle using a single pole magnetic trap. A 28 mm diameter pole made of CMI-C steel is wrapped 550 times with 24-gauge copper wire, turning the pole into an electromagnet. The magnetic pole was connected to a voltage supply (Kepco Power supply, Kepco, Inc., Flushing, NY). The sperm cell was affixed onto a coverslip and the acrosome reaction induced with the addition of ionophore into the flow-cell. Next, the magnetic beads suspended in ASW were introduced into the flow-cell, which was then rocked slowly back and forth to prevent the beads from fast sedimentation, giving enough time for the formation of a biotin–streptavidin bond between the sperm and the beads. We screened for the cells that had a single magnetic bead attached to the acrosome bundles. Once the static image of a bundle was stored, the voltage of the power supply was varied and the images of the deflected bundle at equilibrium were saved. We ensured that the bundle was only elastically deformed, by confirming that the bundle returns to its straight state when the magnetic trap is switched off (see Figure 2(b)).

For calibration of the magnetic force used to deflect the acrosome, we used a suspension of 2.8 μm magnetic beads in 4.95 M $CaCl_2$ at a volume fraction ($\sim 10^{-7}$) at which magnetic and hydrodynamic interactions between beads can be neglected.[18] The same specified voltages used in the experiments were applied and the trajectories of the beads were recorded. The characteristic Reynolds number associated with the bead motion is of the order of 10^{-5}, so that the magnetic force can be estimated directly from the viscous drag force using Stokes formula, $F_m = 6\pi\mu r_p \nu_m$, where μ is the viscosity of 4.95 M $CaCl_2$ solution (9.95×10^{-3} Pa s at 25 °C), r_p is the particle radius, and ν_m is the particle velocity (typically less than 9 μm/s). Since the force is sensitive to the position of the pole relative to the location of the beads, the location of the pole is not disturbed between the measurements and calibration.

Acknowledgements

We thank J. Sutin for help in setting up the magnetic trap. Microscopy was conducted in the W. M. Keck Microscope Facility at the Whitehead Institute. This work was supported by a NSF Graduate Research fellowship (to J.S.), the Center for Biomedical Engineering at MIT (to L.M. and P.M.), NIH GM52703 (to P.M.), and an NIH supplementary grant (to L.M.).

References

1. Kreis, T. & Vale, R. (1999). *Guidebook to the Cytoskeletal and Motor Proteins*, 2nd edit., Sambrook and Tooze Publication at Oxford University Press, Oxford, UK.
2. Tilney, L. G., Tilney, M. S. & Guild, G. M. (1995). F-actin bundles in *Drosophila* bristles. I. Two filament cross-links are involved in bundling. *J. Cell Biol.* **130**, 629–638.
3. Tilney, L. G., Connelly, P., Smith, S. & Guild, G. M. (1996). F-actin bundles in *Drosophila* bristles are assembled from modules composed of short filaments. *J. Cell Biol.* **135**, 1291–1308.
4. Cant, K., Knowles, B. A., Mooseker, M. S. & Cooley, L. (1994). *Drosophila* singed, a fascin homolog, is required for actin bundle formation during oogenesis and bristle extension. *J. Cell Biol.* **125**, 369–380.
5. Matsudaira, P. T. & Burgess, D. R. (1979). Identification and organization of the components in the isolated microvillus cytoskeleton. *J. Cell Biol.* **83**, 667–673.
6. Tilney, M. S., Tilney, L. G., Stephens, R. E., Merte, C., Drenckhahn, D., Cotanche, D. A. & Bretscher, A. (1989). Preliminary characterization of the stereocilia and cuticular plate of hair cells in the chick cochlea. *J. Cell Biol.* **109**, 1711–1723.
7. Tilney, L. G., Tilney, M. S. & DeRosier, D. J. (1992). Actin filaments, stereocilia and hair cells: how cells count and measure. *Annu. Rev. Cell Biol.* **8**, 257–274.

8. Tilney, L. G. (1975). Actin filaments in the acrosomal reaction of *Limulus* sperm. *J. Cell Biol.* **64**, 289–310.
9. Sherman, M. B., Jakana, J., Sun, S., Matsudaira, P., Chiu, W. & Schmid, M. F. (1999). The three-dimensional structure of the *Limulus* acrosomal process—a dynamic actin bundle. *J. Mol. Biol.* **294**, 139–149.
10. Isambert, H., Venier, P., Maggs, A. C., Fattoum, A., Kassab, R., Pantaloni, D. & Carlier, M.-F. (1995). Flexcibility of actin filaments derived from thermal fluctuations. *J. Biol. Chem.* **19**, 11437–11444.
11. Kojima, H., Ishijima, A. & Yanagida, T. (1994). Direct measurement of stiffness of single actin filaments with and without tropomyosin by *in vitro* nanomanipulation. *Proc. Natl Acad. Sci. USA*, **91**, 12962–12966.
12. Xu, J. Y., Wirtz, D. & Pollard, T. D. (1998). Dynamic cross-linking by alpha-actinin determines the mechanical properties of actin filament networks. *J. Biol. Chem.* **273**, 9570–9576.
13. Wachsstock, D. H., Schwarz, W. H. & Pollard, T. D. (1994). Cross-linker dynamics determine the mechanical properties of actin gel. *Biophy. J.* **66**, 801–809.
14. Howard, J. & Ashmore, J. F. (1986). Stiffness of sensory hair bundles in the sacculus of the frog. *Hear. Res.* **23**, 93–104.
15. Schmid, M. F., Agris, J. M., Jakana, J., Matsudaira, P. & Chiu, W. (1994). Three-dimensional structure of a single filament in the *Limulus* acrosomal bundle: scruin binds to homologous helix-loop beta motifs in actin. *J. Cell Biol.* **124**, 341–350.
16. Howard, J. (2000). *Mechanics of Motor Proteins and the Cytoskeleton*, Sinauer Associate, Inc, Sunderland, MA.
17. Gere, J. M. & Timoshenko, S. P. (1990). *Mechanics of Materials*, PWS Publishing Company, Boston, MA.
18. Amblard, F., Yurke, B., Pargellis, A. & Leibler, S. (1996). A magnetic manipulator for studying local rheology and micromechanical properties of biological systems. *Rev. Sci. Instrum.* **67**, 818–827.

Appendix

Solution for the deflection of a non-prismatic rod

Hydrodynamic flow method

The acrosome bundle is modelled as a tapering rod made of n cylinders whose radii, r_n, vary according to the linear function fitted to the slope of the bundle obtained from electron micrographs (Figure A1(a)). The tapering angle and $R_{\min}$ are estimated by taking the average of the tip radii obtained from cross-sectional electron micrographs of 13 different cells. The slope of the bundle is expressed as $S = (R_{\max} - R_{\min})/L_{\text{tot}}$, where L_{tot} is the average total bundle length, 60 μm. The radius is $r_n(x_n) = R_{\text{base}} + S(L/N - x_n)$ with R_{base} being the radius of the bundle at the junction (the clamped boundary) and $x_n = Ln/N$ is the location of the end of each segment where L is the length of the extended bundle. Since the acrosome bundle does not always extend to its full length with its extended length varying from cell to cell ($45 \sim 65$ μm), R_{base} depends on the length of the extended bundle, with $R_{\text{base}} = R_{\min} + L(R_{\max} - R_{\min})/L_{\text{tot}}$.

We assume that each segment in the bundle obeys linear elastic theory, and apply the method of superposition to obtain the total deflection at the tip of the entire bundle.[A1] This method is valid when the material is linear, elastic, and isotropic, and if the deflection and taper are small. As an illustration, consider a cantilever beam (Figure A1(b)) under a distributed load f. The tip deflection $\delta_{\text{tot}} = \delta_{\text{B}} + \delta_{\text{O}} + \theta_{\text{C}}(L/2)$ where δ_{B} is the deflection of the $\overline{AB}$, δ_{O} the deflection of the $\overline{OA}$, and $\theta_{\text{C}}(L/2)$ the transverse displacement due to the rigid body rotation θ_{O} of the boundary A. Using the same principle for a tapering rod made of n cylinders yields the following:

$$\begin{aligned}\delta_n &= \frac{f}{8EI_n}\left(\frac{L}{N}\right)^4 + \frac{M_n}{2EI_n}\left(\frac{L}{N}\right)^2 + \frac{V_n}{3EI_n}\left(\frac{L}{N}\right)^3 \\ &+ \left(\frac{f}{6EI_n}\left(\frac{L}{N}\right)^3 + \frac{M_n}{EI_n}\left(\frac{L}{N}\right) + \frac{V_n}{2EI_n}\left(\frac{L}{N}\right)^2\right) \\ &\times \left(L - \frac{L}{N}n\right),\ n \\ &= 1 : N-1 \\ \delta_N &= \frac{f}{8EI_N}\left(\frac{L}{N}\right)^4, \qquad n = N \end{aligned} \tag{A1}$$

where $M_n = f(L^2 - x_n^2)/2 + fLx_n$ is the moment at the end of nth segment ($x_n = (L/N)n$), $V_n = fL - fx_n$ the shear force at the end of nth segment, and $I_n = \pi(r_n)^4/4$ the moment of inertia for the nth segment. The total deflection is then:

$$\delta_{\text{tot}} = \delta_1 + \delta_2 + \delta_3 + \ldots \delta_N \tag{A2}$$

Equation (A2) yields the Young's modulus E, given the experimentally measured values of δ_{tot}, L, and r_n.

Magnetic trap method

When the distributed hydrodynamic load is replaced by a point load due to the magnetic bead, we find:

$$\begin{aligned}\delta_n &= \frac{M_n}{2EI_n}\left(\frac{a}{N}\right)^2 + \frac{V_n}{3EI_n}\left(\frac{a}{N}\right)^3 \\ &+ \left(\frac{M_n}{EI_n}\left(\frac{a}{N}\right) + \frac{V_n}{2EI_n}\left(\frac{a}{N}\right)^2\right)\left(a - \frac{a}{N}n\right),\ n = 1 \\ &: N-1 \\ \delta_N &= \frac{F_\perp}{3EI_N}\left(\frac{a}{N}\right)^3,\ n = N \end{aligned} \tag{A3}$$

where $M_n = F_\perp(a - x_n)$ and $V_n = F_\perp$. Using equation (A2), we can then determine E, given the experimentally measured values of F_n, δ_{tot}, a.

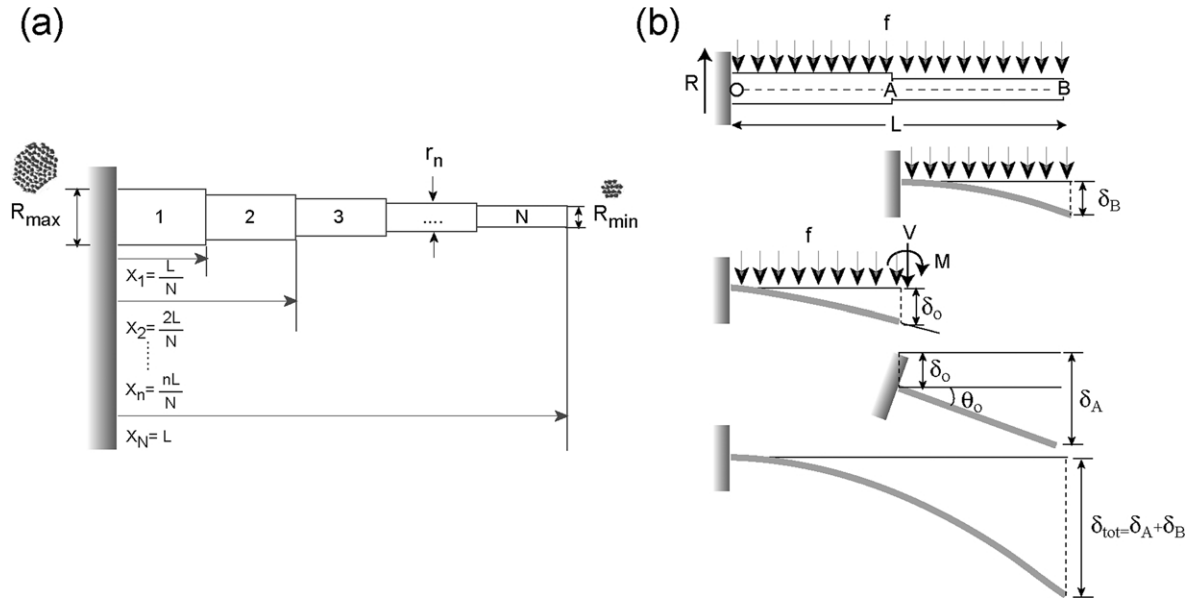

Figure A1. Method of superposition. (a) The acrosomal bundle of horseshoe crab is modelled as a linearly tapering elastic rod made of n cylinders. From electron micrographs of cross-sectional sperm cells, the maximum and minimum radii ($R_{max} \sim 68$ nm and $R_{min} \sim 24$ nm) are measured and the slope S of the taper is calculated to be 7.3×10^{-4}. The radii r_n of each segment vary according to the linear function fitted to the slope of the bundle such that $r_n(x_n) = R_{base} + S(L/N - x_n)$. At two ends of the drawing, the EM images of the negatively stained acrosomal bundle are shown. (b) Cantilever beam with two different moments of inertia is illustrated with the elements contributing to the total deflection with $\delta_{tot} = \delta_A + \delta_B = \delta_B + (\delta_O + \delta\theta_O(L/2))$.

References

A1. Gere, J. M. & Timoshenko, S. P. (1990). *Mechanics of Materials*, PWS Publishing Company, Boston, MA.

Edited by M. Moody

(Received 6 October 2003; received in revised form 29 December 2003; accepted 12 January 2004)